

Expected EDL Navigation Performance with Spacecraft to Spacecraft Radiometric Data

P. Daniel Burkhart*, Todd Ely* and Courtney Duncan*

Jet Propulsion Laboratory, Pasadena, CA, 91107, USA

E. Glenn Lightsey†, Thomas Campbell‡ and Andreas Mogensen‡

The University of Texas at Austin, Austin, TX, 78712, USA

Pinpoint landing (defined for the purpose of this discussion as landing within 1km of a preselected target) is a key Advanced Entry, Descent and Landing (EDL) technology for future Mars landers. Key scientific goals for Mars exploration, such as the search for water and characterization of aqueous processes on Mars, the study of mineralogy and weathering of the Martian surface and the search for preserved biosignatures in Martian rocks, require placing landers at pre-defined locations of greatest scientific interest. The capability to land within 1 km of a pre-defined landing site will improve safety and enable landing within roving range of sites of scientific interest while avoiding hazardous areas. A critical component of the closed-loop guidance, navigation and control (GN&C) system required for pinpoint landing is position and velocity estimation in real time. Spacecraft-to-spacecraft navigation will take advantage of the UHF link between two spacecraft (i.e. to an orbiter from an approaching lander for EDL telemetry relay) to build radiometric data, specifically the total count carrier phase of the Doppler shifted 2-Way coherent UHF signal, that are processed to determine position and velocity in real time. The improved onboard state knowledge provided by spacecraft-to-spacecraft navigation will reduce the landed position error and improve the performance of entry guidance. Results from the first of two years planned for this effort are documented here, including selection and documentation of prototype algorithms that will go forward into flight code along with analysis results used to define the algorithm set.

I. Introduction

PINPOINT landing (defined for the purpose of this discussion as landing within 1km of a preselected target) is a key Advanced Entry, Descent and Landing technology for future Mars landers. Key scientific goals for the next decade of Mars exploration, such as the search for water and characterization of aqueous processes on Mars, the study of mineralogy and weathering of the Martian surface and the search for preserved biosignatures in Martian rocks, requires placing landers at pre-defined locations of greatest scientific interest. The capability to land within 1km of a predefined landing site will improve safety and enable landing within roving range of sites of scientific interest while avoiding hazardous areas. The addition of spacecraft-to-spacecraft navigation data processing onboard the entry body in real time will enable improvements in surface positioning error and improve the performance of entry guidance.

An entry, descent and landing (EDL) system enabling pinpoint landing requires technology beyond that specified for Mars Science Laboratory (MSL), scheduled to launch in 2009. MSL will demonstrate the first required components for pinpoint landing, including closed-loop entry guidance during hypersonic flight.¹ The MSL EDL system does not have the capability to improve the onboard knowledge of the spacecraft

*Senior Staff Engineer, Guidance Navigation and Control Section, 4800 Oak Grove Drive, M/S 301-125L, Senior Member AIAA.

†Associate Professor, Department of Aerospace Engineering and Engineering Mechanics, 1 University Station C0600, Senior Member AIAA.

‡Graduate Student, Department of Aerospace Engineering and Engineering Mechanics, 1 University Station C0600, Student Member AIAA.

position and velocity after entry and before radar altitude and velocity data are available at the beginning of the powered descent phase. Using spacecraft-to-spacecraft navigation to provide this capability is the motivation for this task.

Spacecraft-to-spacecraft navigation for EDL involves forming radiometric data with a radio link using the UHF band (300–3000MHz) between the approaching lander and an orbiting spacecraft, as shown in Figure 1 for MSL. The UHF link will be made between the two spacecraft before atmospheric entry, but the focus of this effort is processing this data after cruise stage separation (roughly 10 minutes before entry). These data are available throughout EDL with the exception of periods during hypersonic flight where the ionizing plasma around the entry body makes closing the communication link difficult. Even with these outages, enough data can be collected and processed onboard in real time to significantly improve the onboard state knowledge during hypersonic flight.²

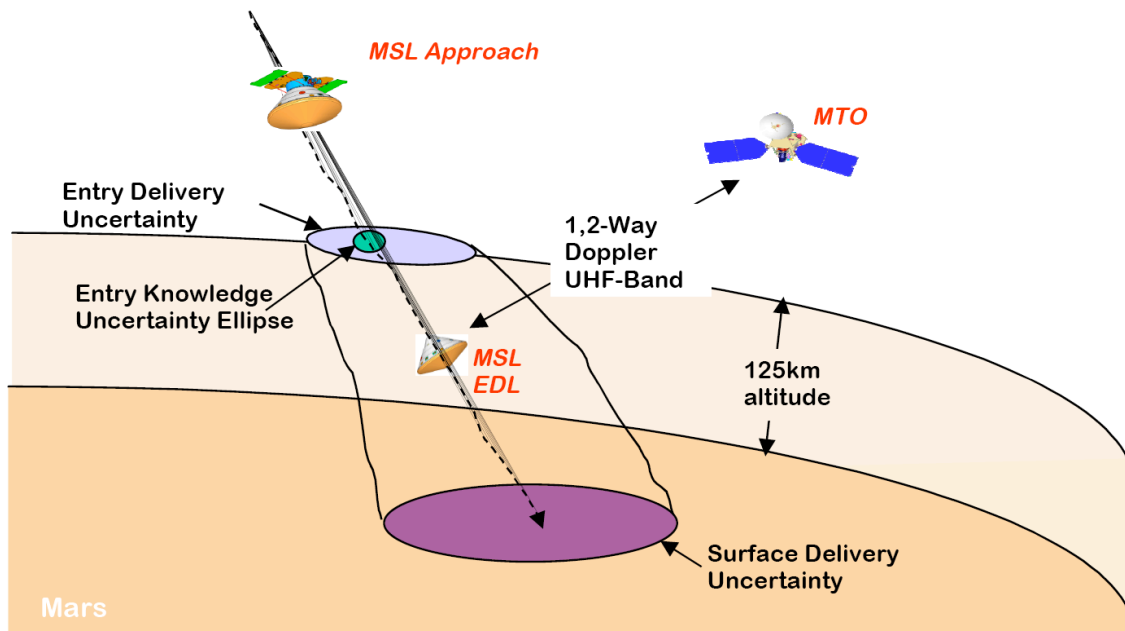


Figure 1. Schematic of spacecraft-to-spacecraft navigation as used for EDL. The entry delivery and knowledge uncertainties for the approaching lander are depicted, as is the surface positioning error. Spacecraft-to-spacecraft navigation data will be processed throughout EDL, including other external sensor data such as radar altimeter measurements.

The Electra Program at JPL has developed and produced a software defined radio (SDR) which is manifested as baseline equipment on future Mars missions beginning with Mars Reconnaissance Orbiter (MRO) scheduled for launch in August 2005. These SDRs are nominally configured for Mars-local UHF operation for data relay in the vicinity of 437MHz and are also capable of making high precision radiometric measurements in Doppler and range.

By design, Electra SDRs have excess computing capacity and memory sufficient for hosting an on board, real time navigation filter. The current Electra design features a space qualified Sparc V-7 processor running at 25MHz and several megabytes of available memory. Over half of each of these resources is available for applications such as real time navigation filtering under direction of the RTEMS (Real-Time Executive for Multiprocessor Systems) operating system. (Electra is a single processor application for RTEMS.)

Utilizing spare Electra capacity for on board navigation frees other resources, such as the main spacecraft housekeeping computer, from involvement in such a computationally intensive, time critical task. Also, the radiometric data is locally available inside Electra and need not be transferred over the spacecraft bus.

In the present work a navigation filter task will be demonstrated on prototype Electra baseband hardware with the goal of showing that Electra resources are sufficient to host a sophisticated navigation algorithm with reasonably low latency in terms of data input to updated state output times.

Competing optical techniques for providing onboard knowledge provide similar accuracy but are more

costly. They require the addition of a camera or cameras to the lander, along with image processing software to generate navigation data. The Electra radio used for spacecraft-to-spacecraft navigation does not add hardware cost as it is already baseline equipment for future Mars landers. In addition, optical systems require performing EDL during daytime at the landing site, and may be further constrained by additional lighting requirements. Spacecraft-to-spacecraft radiometrics do not have these constraints.

II. Scenario Definition

An approach and EDL scenario based on Mars Science Laboratory (MSL) was constructed to quantify the position and velocity knowledge improvements gained by adding spacecraft-to-spacecraft data. This scenario assumes the orbiting spacecraft is Mars Telecommunications Orbiter (MTO) in order to define both an orbit and a relay capability. The scenarios used here will incorporate realistic trajectories for all assets used, including the MSL approach and EDL trajectories and MTO orbits. While MSL is not planning to do pinpoint landing, it does have the required hypersonic guidance that will most likely be used for any future pinpoint landing mission.¹ Since the MSL baseline up to chute deploy is a likely candidate for the hypersonic strategy to be used for pinpoint landing, analysis of the MSL scenario applies to pinpoint landing. Although other entry options are available (including hypersonic guidance approaches not derived from Apollo and higher L/D entry bodies), all will benefit from improved onboard knowledge.

The entry state for the selected MSL trajectory is listed in Table 1. This entry state is the final condition of a valid Earth/Mars transfer trajectory that was used for approach navigation analysis.³ This entry state is also the initial condition that, combined with an assumed entry body size, aeroshell shape and EDL timeline, arrives at a landing site defined at 41.45S latitude, 286.74E longitude. These details that lead to the specific EDL nominal trajectory are not as important to this analysis as the fact that these represent a reasonable MSL trajectory from entry to parachute deploy, or the end of the entry guidance phase.

Table 1. MSL Entry State*, Mars planet centered inertial Mars-mean-equator of epoch 08-OCT-2010 19:06:38.61

Component	Value (km)	Component	Value (km/s)
X	2509.459003	\dot{X}	-1.473129134
Y	377.697451	\dot{Y}	5.335713468
Z	-2442.509568	\dot{Z}	1.264687130

* Entry defined as a radial distance of 3522.2 km from the center of Mars.

For the MSL approach trajectory, analysis consistent with the planned approach navigation strategy and high-fidelity simulation was used.³ The analysis performed here includes Deep Space Network (DSN) radiometric data collected starting 30 days before entry and ending 6 hours before entry, which is the assumed data cutoff for the final onboard state update before entry. A simplified approach filter that has results similar to the reference high-fidelity analysis has been developed. In addition, to quantify the impact of the initial values on the spacecraft-to-spacecraft data processing, a case without DSN data was analyzed.

For the specific entry conditions in Table 1, an MSL EDL trajectory (including position, velocity and attitude) was obtained that is valid through supersonic chute deploy. The models used for the remainder of EDL are not consistent with the MSL plan but a complete trajectory that lands safely was supplied. In order to approximate the trajectory for the entry guidance phase, several simplified models were developed. Instead of the high-fidelity atmosphere used to generate the supplied trajectory, an approximate density profile using an 8-layer exponential atmosphere was created. Simple lift and drag models with single C_L and C_D coefficients were included to model the dynamic effects of the atmosphere instead of an entry body aerodynamics database. The spacecraft attitude is assumed for this analysis to be perfect, although it will be assumed to be directly integrated from inertial measurement unit (IMU) in the prototype flight code. Since there are known limitations to the above models, the filter will estimate both C_L and C_D to improve the post-fit trajectory.

The nominal orbit elements for the telecommunications asset at Mars are shown in Table 2. These elements are proposed for MTO and enable coverage of a large fraction of the surface of Mars, as opposed to a low-altitude science or mapping orbit. In order to understand the impact of the orbit geometry relative to

the approaching lander, the mean anomaly and longitude of node were allowed to vary to achieve overflight of the approach ground track.⁴

Table 2. Nominal orbital elements for the relay orbiter, Mars planet centered inertial Mars-mean-equator of epoch 08-OCT-2010 13:06:38.61

Component	Value	Component	Value (deg)
Semi-Major Axis (km)	8114.6722	Longitude of Node*	293.8104
Eccentricity	0.463566	Argument of Periapsis	132.5908
Inclination (deg)	116.6730	Mean Anomaly*	289.7591

* Parameters were varied to optimize link geometry, nominal values shown.

For the defined MSL arrival trajectory, an orbit crossing by the relay orbiter can be achieved by changing the node to 314° and the mean anomaly to 170° . A groundtrack plot of both spacecraft from separation to landing of the approach vehicle is shown in Figure 2. Note that changing the node moves the ground track along the longitude axis with little change in latitude and modifying the mean anomaly moves the ground track in the latitude direction with small changes in longitude. Note as well that the geometry between the orbiter and the approaching lander is favorable for most orbiter conditions that have visibility. This is due to the large angle between the orbit planes and a significant variation in the relative velocity during the spacecraft-to-spacecraft tracking pass, which improves observability.⁴

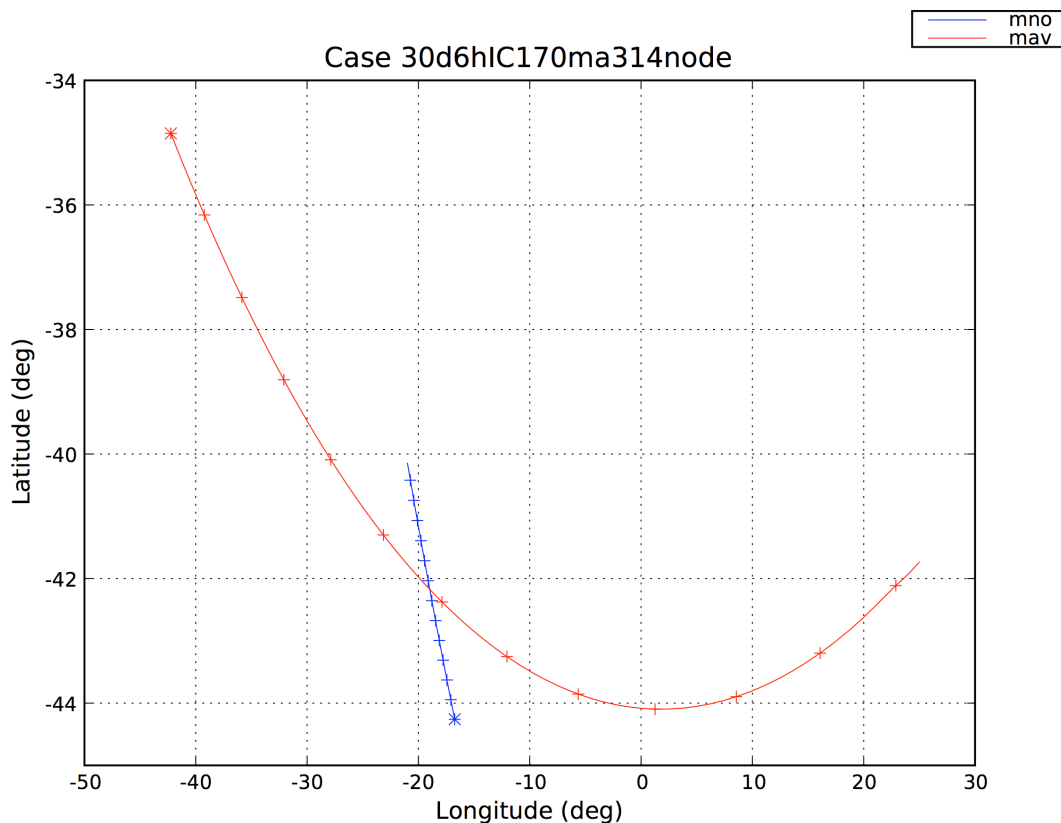


Figure 2. Ground track plot for final 10 minutes of flight for a generic Mars Network orbiter (blue, labeled “mno”) and a Mars approach vehicle (red, labeled “mav”). The starting point is denoted by an \times for each asset with $+$ marks at 1 minute intervals along the trajectory.

III. Covariance Analysis

The first analysis was done assuming DSN tracking of the approaching lander from 30 days before entry to 6 hours before entry, with a single UHF tracking pass beginning about 40 minutes before entry and ending at landing. Results for the final 8 hours before entry is shown in Figure 3. These estimate and covariance values are rotated to Radial-Transverse-Normal (RTN) coordinates, which are defined here as

$$\begin{aligned} \mathbf{R} &= \frac{\mathbf{r}}{|\mathbf{r}|} \\ \mathbf{T} &= \frac{\mathbf{N} \times \mathbf{R}}{|\mathbf{N} \times \mathbf{R}|} \\ \mathbf{N} &= \frac{\mathbf{r} \times \mathbf{v}}{|\mathbf{r} \times \mathbf{v}|} \end{aligned}$$

where \mathbf{r} and \mathbf{v} are the inertial spacecraft position and velocity, respectively, and $|\cdot|$ represents the vector 2-norm. The growth in the radial component is due to covariance propagation correlation effects and process noise after the DSN data ends but before the UHF Doppler collection begins. The other components and the RSS value do not show growth. Note as well the immediate and dramatic decrease in all the position elements when the UHF Doppler data collection begins.

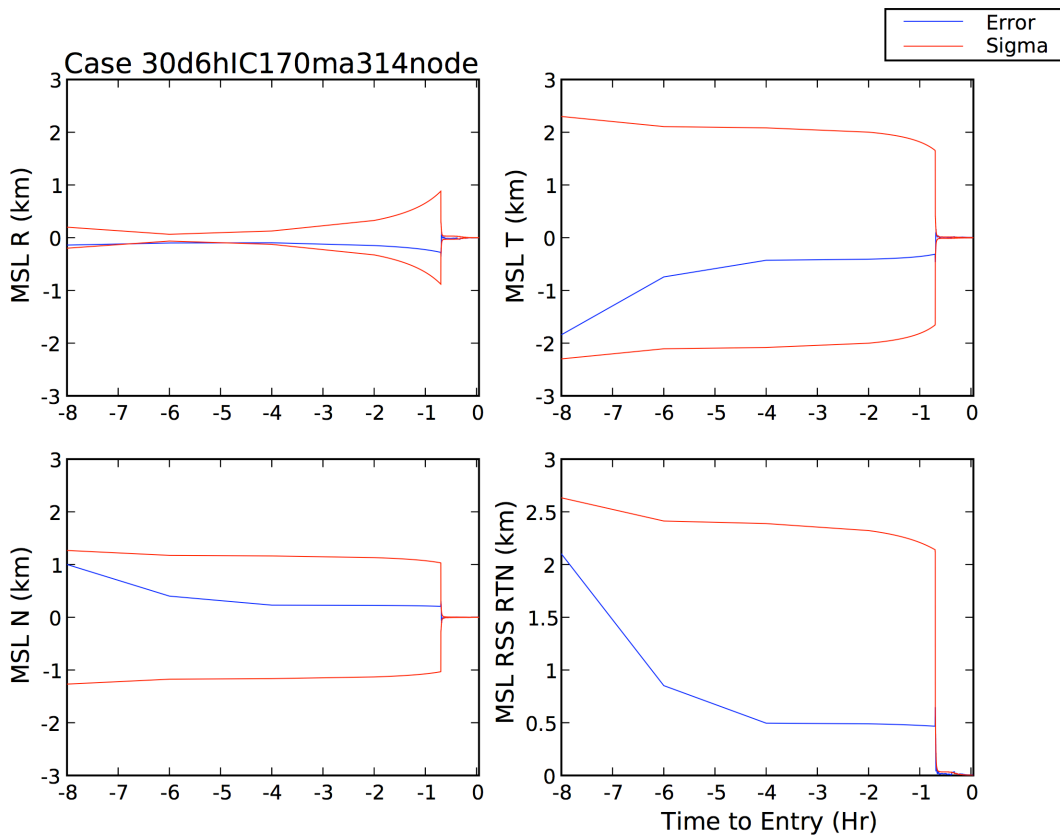


Figure 3. Simulated UHF data processing results with DSN tracking for an MSL approach and landing in Radial (R), Transverse (T) and Normal (N) directions, along with RSS position estimate and 1σ error. Note that DSN tracking ends 6 hours from entry and the resulting error growth in the radial direction. UHF Doppler collection begins 40 minutes from entry.

To better see what is happening in the last hour before entry, a plot that focuses on the last hour for the same case is shown in Figure 4. In focusing on the immediate decrease in the position estimate errors and uncertainties, it is clear that the largest improvement is with the first minutes UHF Doppler data, decreasing from a mapped RSS position error of nearly $2.5km$ to under $100m$ within a few minutes

and decreasing to nearly 10m before entry (defined as $t = 0$ in the figure). These results clearly show the benefits of collecting spacecraft-to-spacecraft UHF Doppler and processing with a fit covariance from DSN radiometric data processing.

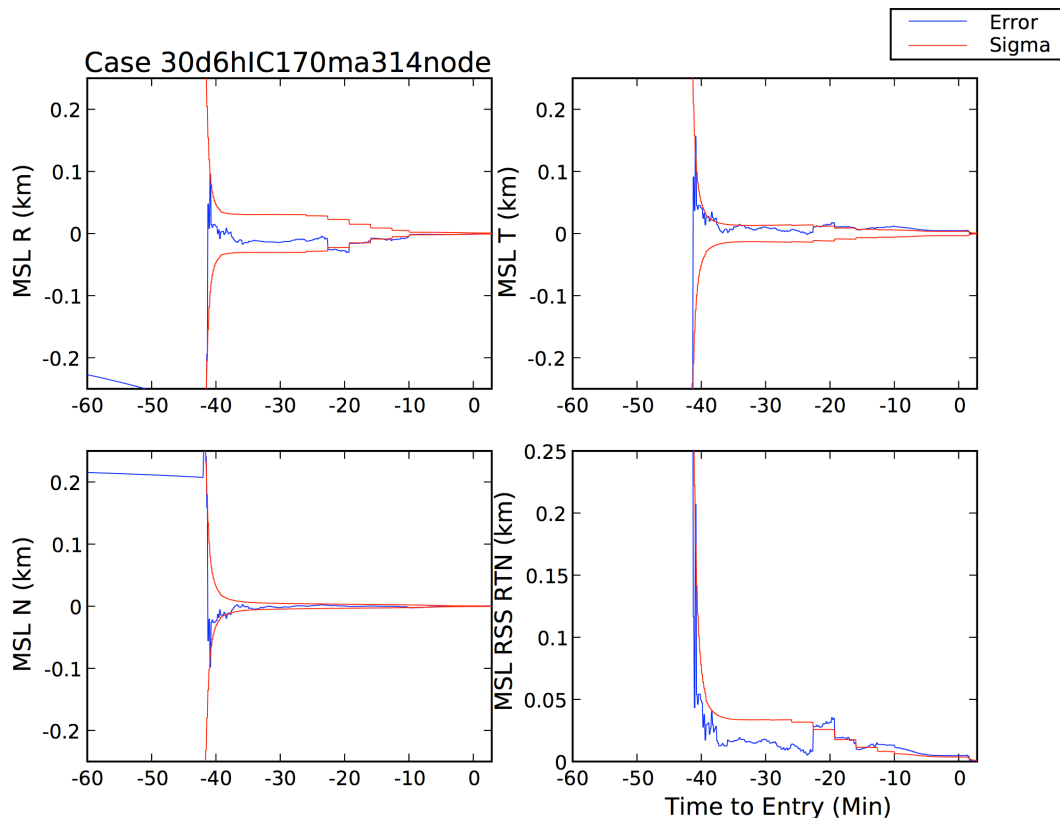


Figure 4. Simulated UHF data processing results with DSN tracking as shown in Figure 3, but focusing on the last hour before entry. Note that with only a few minutes of collecting UHF Doppler the estimates and uncertainties drop below 50m (1σ) and continue to improve as more data are collected.

The second analysis assumes only spacecraft-to-spacecraft data are processed starting at the nominal MSL separation time of 10 minutes before entry interface and ending at chute deploy. The results do not include UHF outages due to plasma, although the results as a function of time can be used to determine the errors at the time of the data outage. The results for this analysis are shown in Figure 5. This case shows the expected result for processing only UHF data after separation and assuming a diagonal initial covariance.

IV. Spacecraft-to-Spacecraft Navigation Algorithms

In order to achieve the goal of having a navigation filter running on the Electra processor, the algorithms required must be defined. The selection of algorithms is separated into three main areas. The first area is dynamic modeling, which includes all forces and moments acting on the spacecraft. The second area is measurement modeling, which includes all incoming data that are to be processed with this filter. The third area is the selection of a filter algorithm. Each of these areas are covered in detail.

A. Dynamic models

There are several options for the level of fidelity in the dynamics model. It is possible to simply integrate the IMU output and only model the gravitational acceleration, but here it is assumed that the accelerometer output is processed as a measurement to update the lander's position and velocity while the gyro output is integrated directly to propagate the attitude.

The filter dynamics model is based on a development of an EDL reconstruction tool for Mars Exploration

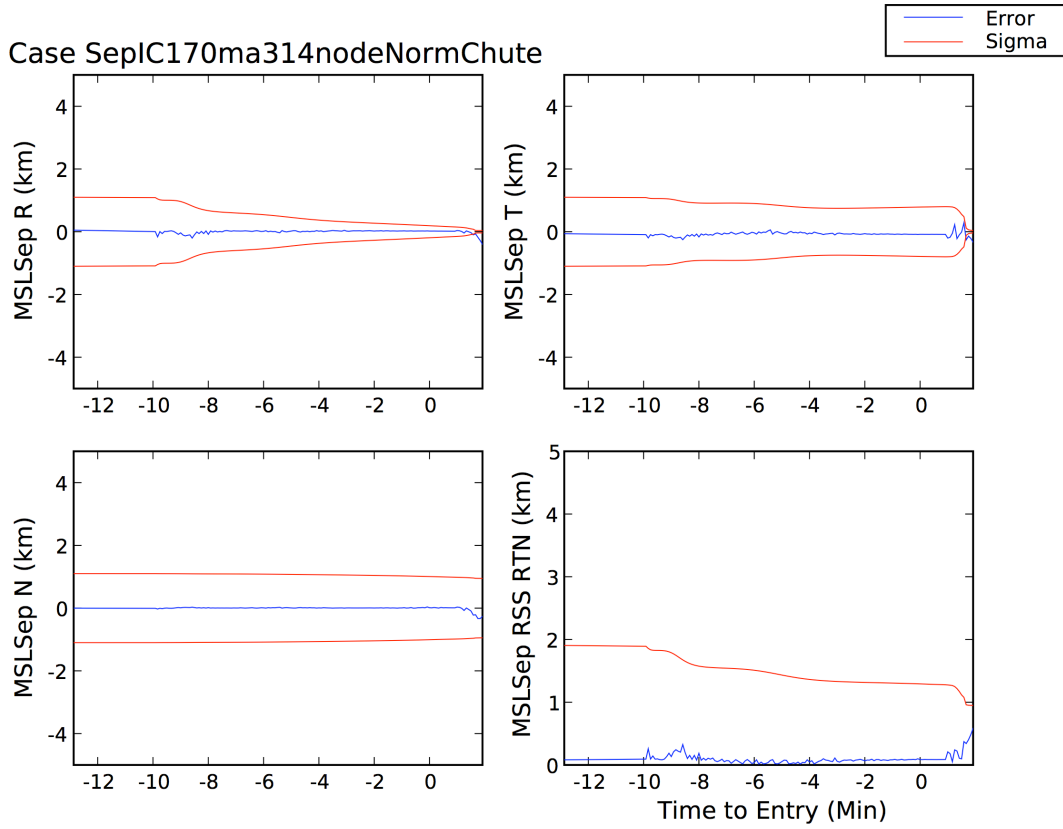


Figure 5. Simulated UHF data processing results for an MSL approach and landing in Radial (R), Transverse (T) and Normal (N) directions, along with RSS position estimate and 1σ error. UHF Doppler collection begins 10 minutes from entry.

Rover (MER) in 2002.⁵ This development is currently being used for an aerobraking analysis tool under development for Mars Reconnaissance Orbiter (MRO) to be used in 2006.⁶ The models in this section are used to propagate the spacecraft state and uncertainties in time.

The state vector at time t_k is defined by

$$\mathbf{X}_{k(9 \times 1)} = \begin{bmatrix} [\mathbf{r}_{cg}]^I & (3 \times 1) \\ [\mathbf{v}_{cg}]^I & (3 \times 1) \\ [\delta \mathbf{a}_{cg,unmod}] & (3 \times 1) \end{bmatrix} = \begin{bmatrix} \text{vehicle c.g. position, planet-centered inertial frame} \\ \text{vehicle c.g. velocity, planet-centered inertial frame} \\ \text{vehicle c.g. unmodeled accelerations, vehicle} \\ \text{c.g.-origin body frame} \end{bmatrix} \quad (1)$$

The equations of motion \mathbf{F}_k for this state vector \mathbf{X}_k and applying the dynamics modeling assumptions above are

$$\mathbf{F}_k = \dot{\mathbf{X}}_{k(9 \times 1)} = \begin{bmatrix} [\dot{\mathbf{r}}_{cg}]^I & (3 \times 1) \\ [\dot{\mathbf{v}}_{cg}]^I & (3 \times 1) \\ [\delta \dot{\mathbf{a}}_{cg,unmod}] & (3 \times 1) \end{bmatrix} = \begin{bmatrix} [\dot{\mathbf{v}}_{cg}]^I \\ \frac{1}{M_{sc}} [\mathbf{F}_{ng,dyn}]^I + \mathbf{T}_B^I [\delta \dot{\mathbf{a}}_{cg,unmod}]^B + [\mathbf{g}_{cg}]^I \\ -[\mathbf{B}_a]_{(3 \times 3)} [\delta \mathbf{a}_{cg,unmod}]_{(3 \times 1)} \end{bmatrix} \quad (2)$$

where

$$[\mathbf{B}_a] = \begin{bmatrix} \frac{1}{\tau_{a_x}} & 0 & 0 \\ 0 & \frac{1}{\tau_{a_y}} & 0 \\ 0 & 0 & \frac{1}{\tau_{a_z}} \end{bmatrix}$$

and

- M_{sc} = vehicle mass
- \mathbf{T}_B^I = rotation matrix, body frame to inertial frame
- $[\mathbf{F}_{ng,dyn}]^I$ = sum of non-gravitational forces acting on body c.g., inertial frame
- $[\delta\mathbf{a}_{cg,unmod}]^B$ = empirically estimated unmodeled accelerations acting at the vehicle c.g., body frame
- $[\mathbf{g}_{cg}]^I$ = gravitational acceleration acting at the body c.g., inertial frame
- τ_{a_n} = unmodeled acceleration component random correlation time constant (sec)

In order to perform time updates on the covariance matrix, a state transition matrix $\Phi_{kk}(t_i, t_{i-1})$ is required. For the state vector \mathbf{X}_k defined above, the state transition matrix is

$$\Phi_{kk}(t_i, t_{i-1}) = \begin{bmatrix} \phi_{rr(3 \times 3)} & \phi_{rv(3 \times 3)} & \phi_{ra(3 \times 3)} \\ \phi_{vr(3 \times 3)} & \phi_{vv(3 \times 3)} & \phi_{va(3 \times 3)} \\ \phi_{ar(3 \times 3)} & \phi_{av(3 \times 3)} & \phi_{aa(3 \times 3)} \end{bmatrix} = \begin{bmatrix} \mathbf{I}_{(3 \times 3)} & \phi_{rv(3 \times 3)} & \phi_{ra(3 \times 3)} \\ \mathbf{0}_{(3 \times 3)} & \mathbf{I}_{(3 \times 3)} & \phi_{va(3 \times 3)} \\ \mathbf{0}_{(3 \times 3)} & \mathbf{0}_{(3 \times 3)} & \mathbf{I}_{(3 \times 3)} \end{bmatrix} \quad (3)$$

where

$$\begin{aligned} \phi_{rv(3 \times 3)} &= \frac{\partial[\mathbf{r}_{cg}]^I(t_i)}{\partial[\mathbf{v}_{cg}]^I(t_{i-1})} = \mathbf{I}_{(3 \times 3)} \Delta t \\ \phi_{ra(3 \times 3)} &= \frac{\partial[\mathbf{r}_{cg}]^I(t_i)}{\partial[\delta\mathbf{a}_{cg,unmod}]^B(t_{i-1})} = \mathbf{T}_{B(3 \times 3)}^I \frac{\Delta t^2}{2} \\ \phi_{va(3 \times 3)} &= \frac{\partial[\mathbf{v}_{cg}]^I(t_i)}{\partial[\delta\mathbf{a}_{cg,unmod}]^B(t_{i-1})} = \mathbf{T}_{B(3 \times 3)}^I \Delta t \end{aligned}$$

B. IMU Measurements

The IMU measurement model is based on a development of an EDL reconstruction tool for Mars Exploration Rover (MER) in 2002.⁵ This development is currently being used for an aerobraking analysis tool under development for Mars Reconnaissance Orbiter (MRO) to be used in 2006.⁶ The IMU data includes output from 3 orthogonal gyros and 3 orthogonal accelerometers for the approaching lander. The models here are based on the current data processing strategy, which is still under development. This strategy is to process the IMU output via filtering of the accelerometer measurements to update the position and velocity and to directly integrate the gyro measurements to update attitude.

The model used to create the gyro measurements from the true body angular rates is

$$\boldsymbol{\omega}_{G(3 \times 1)} = \mathbf{M}_{SF_g(3 \times 3)} \left\{ \mathbf{I}_{(3 \times 3)} + \mathbf{M}_{MA_g(3 \times 3)} + \mathbf{M}_{NO_g(3 \times 3)} \right\} \left\{ \mathbf{T}_{B(3 \times 3)}^G [\boldsymbol{\omega}_{SC(3 \times 1)}]^B \right\} + \mathbf{b}_{g(3 \times 1)} + \boldsymbol{\epsilon}_{g(3 \times 1)} \quad (4)$$

where

- $\boldsymbol{\omega}_G$ = Angular rates measured by gyro, in gyro platform frame
- \mathbf{M}_{SF_g} = 3×3 matrix of gyro scale factor errors (diagonal matrix)
- \mathbf{M}_{MA_g} = 3×3 matrix of gyro axis misalignment errors (zero-diagonal matrix)
- \mathbf{M}_{NO_g} = 3×3 matrix of gyro non-orthogonality errors (zero-diagonal matrix)
- \mathbf{T}_B^G = 3×3 matrix transforming from the body frame to the gyro platform frame
- $[\boldsymbol{\omega}_{SC(3 \times 1)}]^B$ = 3×1 vehicle angular rate, body frame
- \mathbf{b}_g = 3×1 vector of gyro biases, per axis
- $\boldsymbol{\epsilon}_g$ = 3×1 vector of random gyro noise

To define the accelerometer measurement, a brief description of the problem is required. An accelerometer can only sense non-conservative forces and requires outside models for conservative forces to define the total acceleration. For this problem, the only conservative force is gravity. At a minimum, a gravity model is required to directly integrate the data to correctly propagate the trajectory. Since this setup involves filtering the accelerometer data, additional models are required to allow the filter to apply corrections to specific physical models and the remaining unmodeled acceleration parameters. The model used to create the accelerometer measurements from the true non-gravitational acceleration is

$$\mathbf{a}_{a(3 \times 1)} = \mathbf{M}_{SF_a(3 \times 3)} \left\{ \mathbf{I}_{(3 \times 3)} + \mathbf{M}_{MA_a(3 \times 3)} + \mathbf{M}_{NO_a(3 \times 3)} \right\} \left\{ \mathbf{T}_{B(3 \times 3)}^a \left[\mathbf{a}_{a(3 \times 1)} \right]^B \right\} + \mathbf{b}_{a(3 \times 1)} + \boldsymbol{\epsilon}_{a(3 \times 1)} \quad (5)$$

where

$$\begin{aligned} \mathbf{a}_a &= \text{Specific force measured by accelerometer "triad", in accel platform frame} \\ \mathbf{M}_{SF_a} &= 3 \times 3 \text{ matrix of accel scale factor errors (diagonal matrix)} \\ \mathbf{M}_{MA_a} &= 3 \times 3 \text{ matrix of accel axis misalignment errors (zero-diagonal matrix)} \\ \mathbf{M}_{NO_a} &= 3 \times 3 \text{ matrix of accel non-orthogonality errors (zero-diagonal matrix)} \\ \mathbf{T}_B^a &= 3 \times 3 \text{ matrix transforming from the body frame to the accel platform frame} \\ \left[\mathbf{a}_{a(3 \times 1)} \right]^B &= 3 \times 1 \text{ vehicle specific force, body frame} \\ \mathbf{b}_a &= 3 \times 1 \text{ vector of accel biases, per axis} \\ \boldsymbol{\epsilon}_a &= 3 \times 1 \text{ vector of random accel noise} \end{aligned}$$

For $\left[\mathbf{a}_{a(3 \times 1)} \right]^B$,

$$\begin{aligned} \left[\mathbf{a}_{a(3 \times 1)} \right]^B &= \left\{ \mathbf{T}_{I(3 \times 3)}^B \left[\mathbf{a}_{cg,ng,mod(3 \times 1)} \right]^I \right\} + \left[\delta \mathbf{a}_{cg,unmod(3 \times 1)} \right]^B \\ &\quad + \left\{ \left[\boldsymbol{\omega}_{SC(3 \times 1)} \right]^B \times \left[\boldsymbol{\omega}_{SC(3 \times 1)} \right]^B \times \left[\mathbf{r}_{a/cg(3 \times 1)} \right]^B \right\} \\ &\quad + \left\{ \left\{ \left[\boldsymbol{\alpha}_{SC,mod(3 \times 1)} \right]^B + \left[\boldsymbol{\alpha}_{SC,unmod(3 \times 1)} \right]^B \right\} \times \left[\mathbf{r}_{a/cg(3 \times 1)} \right]^B \right\} \end{aligned}$$

where

$$\begin{aligned} \mathbf{T}_I^B &= \text{Transformation matrix, inertial frame to body frame} \\ \left[\mathbf{a}_{cg,ng,mod(3 \times 1)} \right]^I &= \text{Acceleration of the vehicle c.g. due to modeled non-gravitational forces, inertial frame} \\ \left[\delta \mathbf{a}_{cg,unmod(3 \times 1)} \right]^B &= \text{Unmodeled acceleration of the vehicle c.g., body frame} \\ \left[\boldsymbol{\omega}_{SC(3 \times 1)} \right]^B &= \text{Angular velocity of the vehicle, body frame} \\ \left[\mathbf{r}_{a/cg(3 \times 1)} \right]^B &= \text{Distance vector from vehicle c.g. to accelerometer "triad origin" reference point, body frame} \\ \left[\boldsymbol{\alpha}_{SC,mod(3 \times 1)} \right]^B &= \text{Angular acceleration of the vehicle due to modeled torques, body frame} \\ \left[\boldsymbol{\alpha}_{SC,unmod(3 \times 1)} \right]^B &= \text{Unmodeled angular acceleration of the vehicle, body frame} \end{aligned}$$

The measurement partials used to process the accelerometer measurements \mathbf{H}_A are a simplified version of the model used to simulate the measurements. First, the accelerometer reports unbiased non-gravitational

forces, so $\mathbf{b}_a = 0$. In addition, the scale factor error \mathbf{M}_{SF_a} , misalignment error \mathbf{M}_{MA_a} and non-orthogonality error \mathbf{M}_{NO_a} are all zero. With these assumptions, the accelerometer measurement partials are

$$\begin{aligned} \mathbf{H}_{A_{(3 \times 9)}} &= \frac{\partial \mathbf{T}_B^a [\mathbf{a}_a]^B}{\partial \mathbf{X}_k} = \mathbf{T}_B^a \frac{\partial [\mathbf{a}_a]^B}{\partial \mathbf{X}_k} \\ &= \mathbf{T}_B^a \left\{ \frac{\partial [\mathbf{a}_a]^B}{\partial [\mathbf{r}_{cg(3 \times 3)}]^I} \middle| \frac{\partial [\mathbf{a}_a]^B}{\partial [\mathbf{v}_{cg(3 \times 3)}]^I} \middle| \frac{\partial [\mathbf{a}_a]^B}{\partial [\delta \mathbf{a}_{cg, unmod(3 \times 3)}]^B} \right\} \end{aligned}$$

where

$$\begin{aligned} \frac{\partial [\mathbf{a}_a]^B}{\partial [\mathbf{r}_{cg(3 \times 3)}]^I} &= \left\{ \mathbf{T}_I^B \frac{1}{M_{sc}} \left[\frac{\partial [\mathbf{F}_{ng, dyn}]^I}{\partial [\mathbf{r}_{cg}]^I} \right] \right\} + \left\{ \mathcal{R}_{a/cg(3 \times 3)} \{\mathbf{I}_{sc}\}^{-1} \mathbf{T}_I^B \left[\frac{\partial [\boldsymbol{\tau}_{dyn}]^I}{\partial [\mathbf{r}_{cg}]^I} \right] \right\} \\ \frac{\partial [\mathbf{a}_a]^B}{\partial [\mathbf{v}_{cg(3 \times 3)}]^I} &= \left\{ \mathbf{T}_I^B \frac{1}{M_{sc}} \left[\frac{\partial [\mathbf{F}_{ng, dyn}]^I}{\partial [\mathbf{v}_{cg}]^I} \right] \right\} + \left\{ \mathcal{R}_{a/cg(3 \times 3)} \{\mathbf{I}_{sc}\}^{-1} \mathbf{T}_I^B \left[\frac{\partial [\boldsymbol{\tau}_{dyn}]^I}{\partial [\mathbf{v}_{cg}]^I} \right] \right\} \\ \frac{\partial [\mathbf{a}_a]^B}{\partial [\delta \mathbf{a}_{cg, unmod(3 \times 3)}]^B} &= \mathbf{I}_{(3 \times 3)} \end{aligned}$$

with the 3×3 matrix $\mathcal{R}_{a/cg}$ an expansion of the cross-product operator:

$$\mathcal{R}_{a/cg} = \text{“} \times [\mathbf{r}_{a/cg}]^B \text{”} = \begin{bmatrix} 0 & (z_{a/cg})^B & (-y_{a/cg})^B \\ (-z_{a/cg})^B & 0 & (x_{a/cg})^B \\ (y_{a/cg})^B & (-x_{a/cg})^B & 0 \end{bmatrix}$$

C. Electra Measurements

A key radiometric observable that the Electra transceiver will formulate is 2-Way Total Count Carrier Phase O^{2WTP} at the UHF band. This observable contains information that can be related to the 2-Way Integrated Doppler O^{2WID} shift between an Electra transceiving element and a transponding element (typically another Electra). The following provides the mathematical basis for formulating,

1. 2-Way Total Count Carrier Phase O^{2WTP} measurement,
2. 2-Way Integrated Doppler O^{2WID} measurement,

using a detailed model of the Electra transceiving and transponding elements and the Electra clock that is used to time tag the measurements.

1. Electra Oscillator and Clock Models

Electra's signal and clock functions are derived from a common reference oscillator that nominally operates at $76MHz$. Each of the observables $O(\cdot)$ mentioned above is measured and stamped with a time tag derived from a local clock $\tau(t)$ that is being driven by an oscillator that is common to both this clock and the observable. The model for the Electra clock $\tau(t)$ and associated reference oscillator frequency $f(t)$ take the form,

$$\begin{aligned} \tau(t) &= b + (1 + d)t + a \frac{t^2}{2} + \frac{4}{f_0} \psi(t) \quad (\text{s}) \rightarrow \\ f(t) &= f_0 \frac{d\tau}{dt} = f_0 \left[(1 + d) + at + \frac{1}{f_0} \frac{d\psi(t)}{dt} \right] \quad (\text{Hz}), \end{aligned} \tag{6}$$

where

$$\begin{aligned}
t &= \text{true time in seconds past a specified epoch} \\
b &= \text{clock bias (s)} \\
d &= \text{clock drift, or oscillator fractional frequency offset (s/s)} \\
\dot{d} &= \text{clock acceleration, or oscillator aging (s/s}^2\text{)} \\
\psi(t) &= \text{oscillator random phase process in (cycles) with } E[\psi(t)] = 0 \\
f_0 &= \text{Nomonal reference oscillator frequency} = 76728576.15\text{Hz}
\end{aligned}$$

where the appearance of the 4 in the equation for $\tau(t)$ is because the frequency used for the clock divides down the reference oscillator by 4 yielding a nominal clock tick of $52.1318\mu\text{sec}$. Associated with the clock model is the delta clock model which is defined as

$$\Delta t \triangleq \tau(t) - t = b + dt + a\frac{t^2}{2} + \frac{1}{f_0}\psi(t) \quad (\text{s}). \quad (7)$$

It is assumed that there exist nominal model values for the bias, drift, and acceleration ($\bar{b}, \bar{d}, \bar{a}$) that are related to the true values as follows,

$$\begin{aligned}
b = \bar{b} + \delta b &= \text{nominal bias} + \text{an unknown delta bias,} \\
d = \bar{d} + \delta d &= \text{nominal drift} + \text{an unknown delta drift,} \\
a = \bar{a} + \delta a &= \text{nominal acceleration} + \text{an unknown delta acceleration.}
\end{aligned}$$

Using the nominal values any recorded time tag $\tau(t)$ can be calibrated to produce a new time tag as follows,

$$\tau_c(t) = \tau(t) - \Delta\bar{t} = t + \Delta t - \Delta\bar{t} \quad (8)$$

where $\Delta\bar{t}$ is Eq. 7 evaluated with nominal values. The calibrated time tag can be rewritten as follows,

$$\tau_c(t) = \Delta\tau + t$$

with

$$\Delta\tau \triangleq \delta b + \delta d t + \delta a \frac{t^2}{2}.$$

The preceding observations about time tags can be used to expand models for observables that have time been measured and tagged with a local clock. In particular, the measured observable $O^m(\cdot)$ taken at the true time t is dependent on the clock/oscillator parameters as follows,

$$O^m(t; b, d, a),$$

however, note that t is unknown, and that the measurement process has tagged the recorded data with $\tau(t)$. The computed observable $O^c(\cdot)$ is derived from nominal model values and uses the associated time tag τ . The functional form of $O^c(\cdot)$ is,

$$O^c(\tau; \bar{b}, \bar{d}, \bar{a}), \quad (9)$$

The time tag $\tau(t)$ can be calibrated using Eq. 8 which transforms Eq. 9 into,

$$O^c(\tau_c; \bar{b}, \bar{d}, \bar{a}).$$

Now expand $O^m - O^c$ in a Taylor series,

$$\begin{aligned}
O^m(t; b, d, a) - O^c(\tau_c; \bar{b}, \bar{d}, \bar{a}) &= O^m(\tau_c - \Delta\tau; \bar{b} + \delta b, \bar{d} + \delta d, \bar{a} + \delta a) - O^c(\tau_c; \bar{b}, \bar{d}, \bar{a}) \\
&= \left[\frac{\partial O}{\partial b} + \frac{\partial O}{\partial t} \frac{\partial(-\Delta\tau)}{\partial b} \right]_{\tau_c; \bar{b}, \bar{d}, \bar{a}} \delta b + \\
&= \left[\frac{\partial O}{\partial d} + \frac{\partial O}{\partial t} \frac{\partial(-\Delta\tau)}{\partial d} \right]_{\tau_c; \bar{b}, \bar{d}, \bar{a}} \delta d + \\
&= \left[\frac{\partial O}{\partial a} + \frac{\partial O}{\partial t} \frac{\partial(-\Delta\tau)}{\partial a} \right]_{\tau_c; \bar{b}, \bar{d}, \bar{a}} \delta a.
\end{aligned}$$

Note the following

$$\left. \frac{\partial(-\Delta\tau)}{\partial b} \right|_{\tau_c; \bar{b}, \bar{d}, \bar{a}} = \frac{\partial}{\partial b} \left[(b - \bar{b}) + \delta dt + \delta a \frac{t^2}{2} \right]_{\tau_c; \bar{b}, \bar{d}, \bar{a}} = -1$$

likewise,

$$\left. \frac{\partial(-\Delta\tau)}{\partial d} \right|_{\tau_c; \bar{b}, \bar{d}, \bar{a}} = -\tau_c \quad \text{and} \quad \left. \frac{\partial(-\Delta\tau)}{\partial a} \right|_{\tau_c; \bar{b}, \bar{d}, \bar{a}} = -\frac{\tau_c^2}{2}.$$

The preceding observations will be used to derive partials for the observables that are formulated in this study.

2. 2-Way Total Count Phase

The physical path of the signal that is measured by the receiving element of the Electra transceiver at time t_3 originated from the transceivers transmitting element a round trip light time ago plus some hardware delays at time t_1 . The time line of this journey is illustrated in Figure 6 where the following definitions apply,

- t_1 = The time that the signal leaves the transceiver electronics
- t_{1x} = The time that the signal leaves the antenna of the transceiving element. Note that the transceiver delay is defined as $\Delta_{xx} \triangleq t_{1x} - t_1$.
- t_{2r} = The time that the signal is received by the transponding antenna
- t_2 = The time that the transponding NCO actually measures the phase.
- t_{2x} = The time that the signal leaves the antenna of the transponding element. Note that the transponder receive delay is defined as $\Delta_{tr} \triangleq t_2 - t_{2r}$ and the transponder transmit delay is defined as $\Delta_{tx} \triangleq t_{2x} - t_2$. The time between when the NCO measures the phase and when the D/A converter remodulates that phase onto the return carrier is assumed to be negligible.
- t_{3r} = The time that the signal is received at the transceiving antenna.
- t_3 = The time that the transceiving NCO actually measures the phase. Note that the transceiver transmit delay is defined as $\Delta_{xr} \triangleq t_3 - t_{3r}$.
- ρ_1 = $t_{2r} - t_{1x}$ = One-way light time on the forward link from the transceiver to the transponder.
- ρ_2 = $t_{3r} - t_{2x}$ = One-way light time on the return link from the transponder to the transceiver.

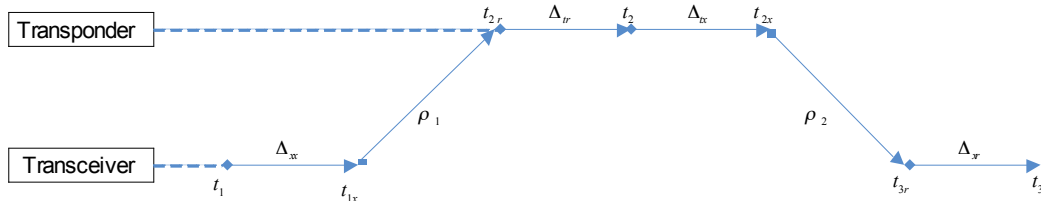


Figure 6. Timeline of an Electra 2-Way total count phase measurement.

With all of these times defined the actual 2-Way total count phase measurement that is recorded by the Electra transceiver can be modeled using,

$$O^{2WTP}(t) \triangleq M_2(\phi_{xx}(t_1) - \phi_{tr}(t_2)) + (\phi_{tx}(t_2) - \phi_{xr}(t_3)), \quad (10)$$

where $\phi_x(\cdot)$ is the phase transceiver at different times at points in the receive/transmit path, and $\phi_t(\cdot)$ is the phase of the transponder at different times and points in its receive/transmit path. The details of these

phase models are described shortly. First, consider that the phase models for the reference oscillator on the transceiver is related to the frequency model given in Eq 6 as follows,

$$\phi_x(t) = \int f_x(t)dt = \phi_{x0} + f_0 \left[(1 + d_x)t + a_x \frac{t^2}{2} \right] + \psi_x(t), \quad (11)$$

where the subscript ‘ x ’ refers to the transceiver, and ϕ_{x0} is the initial phase of the transceiver oscillator. An equivalent model for the transponders reference oscillator takes the form,

$$\phi_t(t) = \int f_t(t)dt = \phi_{t0} + f_0 \left[(1 + d_t)t + a_t \frac{t^2}{2} \right] + \psi_t(t), \quad (12)$$

Where the subscript ‘ t ’ refers to the transponder, and ϕ_{t0} is the initial phase of the transponder oscillator. The components appearing in Eq. 10 can now be defined and related to the oscillator models given by Eqs. 11 and 12, specifically,

$$\phi_{xx}(t) = M_{xx}\phi_x(t) = \text{Phase of the transmitted carrier signal sent by the transceiver at time } t. \quad (13)$$

$$\phi_{tr}(t) = M_{tr}\phi_t(t) = \text{Phase of the transponder signal that is mixed with the received signal at } t. \quad (14)$$

$$\phi_{tx}(t) = M_{tx}\phi_t(t) = \text{Phase of the transponder carrier signal sent by the transponder at time } t. \quad (15)$$

$$\phi_{xr}(t) = M_{xr}\phi_x(t) = \text{Phase of the transceiver signal that is mixed with the received signal at } t. \quad (16)$$

Hence, the signal that the transponder phase tracking loop records, which is then remodulated on the return link signal, is the beat signal obtained via mixing and sampling and is the term $\phi_{xx}(t_1) - \phi_{tr}(t_2)$ in Eq. 10. The remodulated signal is multiplied up by the turnaround ratio M_2 and is related to the other transponder multipliers as follows,

$$M_2 \equiv \frac{M_{tx}}{M_{tr}} \quad (17)$$

Finally, the signal that is ultimately recorded by the transceiving element at the final return of the signal at time t_3 includes the sum of the forward link phase shift $M_2(\phi_{xx}(t_1) - \phi_{tr}(t_2))$ and the return link phase shift given by $\phi_{tx}(t_2) - \phi_{xr}(t_3)$. All of the multipliers in Electra can be set/reset via commanding. Typical values that have been used for simulation are,

$$M_{xx} = 5.6973684210526319$$

$$M_{xr} = 5.2342836257309946$$

$$M_{tx} = 5.2339181286549712$$

$$M_{tr} = 5.6970029239766085$$

and are rational numbers relating to internal integer multipliers that configure Electras transmit and receive frequencies that depend on whether Electra is transceiving or transponding.

Combining Eqs. 11, 12, 13, 14, 15, 16, and 17 and reducing to a numerically stable form yields an simplified expression for Electra’s 2-Way total count phase,

$$\phi^{2WTP}(t_3) = f_0 \left\{ \begin{array}{l} -M_2M_{xx} \left[(1 + d_x)\Delta_T + a_x\Delta_T \left(t_3 - \frac{\Delta_T}{2} \right) \right] \\ + (M_2M_{xx} - M_{xr}) \left[(1 + d_x)t_3 + a_x \frac{t_3^2}{2} \right] \\ + (M_2M_{xx}\psi_x(t_1) - M_{xr}\psi_x(t_3)) - N \end{array} \right\} \quad (18)$$

where,

$$\Delta_T \equiv \Delta_{tr} + \Delta_{tx} + \Delta_{xr} + \Delta_{xx} + \rho_1 + \rho_2. \quad (19)$$

It should be noted that the term for the initial phase has been grouped into an initial phase term labeled N that is typically unknown. The most significant observation regarding Eq. 18 is that the random phase of the transponder oscillator does not appear in the final result. The absence of this random phase contribution is the chief advantage of using two-way data over one-way data. To actually use this data for navigation partial derivatives with respect to dynamic and bias parameters is needed. For the sake of brevity these have not been included in the paper, however, if the reader desires they can contact the authors to obtain them.

3. 2-Way Integrated Doppler

Recall that the 2-Way Total Count Phase measurement $O^{2WTP}(t)$ contains unknown biases. To eliminate these unknowns for navigation the phase measurements are usually processed as an integrated Doppler measurement that is the difference of two phase measurements separated by a specified count time T . That is, the equation defining Electra's 2-Way Integrated Doppler is given by,

$$O^{2WID}(t_3) \triangleq - \{ \phi^{2WTP}(t_3^2) - \phi^{2WTP}(t_3^1) \},$$

where $T \approx t_3^2 - t_3^1$ which is approximate because the Electra clock will drift from the ideal count time T as the real clock progresses from t_3^1 to t_3^2 . It is for this reason that the observable is not divided by the measured count time, as doing so would unnecessarily complicate the partials for the observable.

D. Filter Algorithm

There are several filtering approaches under consideration in cooperation with other technology tasks, but the approach investigated here is the use of an Extended Kalman Filter (EKF).⁸ Various factorized Kalman filter formulations are being studied, along with a sigma-point filter as an alternative.⁹ The formulation of the EKF is based on the square-root implementation by Carlson.¹⁰

V. Future Work

The mathematical models described above will form the basis of a navigation filter that can process IMU and Electra Doppler data. Coding for this filter is in progress and will be completed as part of this task. As this filter is tested, additional modifications to the algorithm set will be provided as needed.

The navigation filter will be ultimately tested on a breadboard version of the Electra processor, which will process Doppler data that will ultimately be built by Electra and IMU data that is received from outside Electra. In preparation for testing in hardware, a software emulator of the Electra SPARC processor, a Sparc V7 RISC based processor with a clock speed of 24MHz, has been obtained. This emulator is a software equivalent of the Electra hardware processor provided by the Electra development team. It will also include the interfaces needed to import the IMU data and to export filtered solutions.

To support hardware testing of the developed filter, a breadboard version of Electra made with commercial parts has been constructed by the Electra team. This breadboard will serve as a demonstration platform for the completed software.

VI. Acknowledgments

The lead author would first like to acknowledge the contributions of the coauthors of this paper. The success of this task is the direct result of their efforts. The authors would also like to thank Tom Jedrey and his team in the Wireless Communications Group at the Jet Propulsion Laboratory for their efforts in supporting this task from the Electra radio side, along with Mike Lisano and Moriba Jah for use of their work as a starting point for the filter algorithms.

This research was carried out at the Jet Propulsion Laboratory, California Institute of Technology, under a contract with the National Aeronautics and Space Administration.

Reference herein to any specific commercial product, process, or service by trade name, trademark, manufacturer, or otherwise, does not constitute or imply its endorsement by the United States Government or the Jet Propulsion Laboratory, California Institute of Technology.

References

¹Mendeck, G. F. and Karman, G. L., "Guidance Design for Mars Smart Landers Using The Entry Terminal Point Controller," *Proceedings of the AIAA Atmospheric Flight Mechanics Conference and Exhibit*, AIAA-2002-4502, Monterey, California, Aug. 5-8, 2002.

²Crain, T. P. and Bishop, R. H., "Mars Entry Navigation: Atmospheric Interface through Parachute Deploy," *Proceedings of the AIAA Atmospheric Flight Mechanics Conference and Exhibit*, AIAA-2002-4501, Monterey, California, Aug. 5-8, 2002.

³Burkhart, P. D., "Approach Navigation for the 2009 Mars Large Lander," *Advances in the Astronautical Sciences, Volume 114*, Univelt, San Diego, CA, 2003, pp. 2183-2198, also AAS Paper 03-250, Jan. 2003.

⁴Ely, T. A. and Guinn, J. R., "Mars Approach Navigation using Mars Network based Doppler Tracking," *Proceedings of the AIAA/AAS Astrodynamics Specialist Conference and Exhibit*, AIAA-2002-4816, Monterey, California, Aug. 5-8, 2002.

⁵Lisano, M., "Interim Planetary Atmosphere Navigation for Estimation and Mission Analysis (IPANEMA) Algorithm Design Document, version 1.0," Draft document, June 2002.

⁶Jah, M. K., Lisano, M. E., Born, G. H., and Axelrad, P., "Mars Aerobraking Spacecraft State Estimation By Processing Inertial Measurement Unit Data," Nasa/tp-2005-213901, Aug. 2005.

⁷Ely, T. A., "Mars Network Observable Models," Jpl iom, 2004.

⁸Gelb, A., *Applied Optimal Estimation*, The MIT Press, 1992.

⁹Julier, S. J. and Uhlmann, J. K., "A New Extension of the Kalman Filter to Nonlinear Systems," *Proceedings of SPIE - The International Society for Optical Engineering*, Vol. 3068, 1997, pp. 182-193, April 21-14, 1997, Orlando, FL.

¹⁰Carlson, N. A., "Federated Square Root Filter for Decentralized Parallel Processes," *IEEE Transactions on Aerospace and Electronic Systems*, Vol. 26, No. 3, 1990, pp. 517-525.